

Pressure tunable magnetic skyrmion phase in $Co_8Zn_8Mn_4$ single crystals

Zhun Li(李准), Xinrun Mi(米薪润), Xinmin Wang(王欣敏), Jian Lyu(吕坚), Na Su(苏娜), Aifeng Wang(王爱峰), Yisheng Chai(柴一晟), Bao Yuan(袁宝), Wanju Luo(罗万居), Hui Cheng(程辉), Jianxiang Gao(高健翔), Hongliang Wang(王洪亮), Lijie Hao(郝丽杰), Mingquan He(何明全), Junying Shen(沈俊英), Young Sun(孙阳), and Xin Tong(童欣)

Citation: Chin. Phys. B, 2026, 35 (**8**): 086103. DOI: 10.1088/1674-1056/ae13ed
http://cpb.iphy.ac.cn; http://iopscience.iop.org/cpb

What follows is a list of articles you may be interested in

First-principles prediction of phase transformation and mechanical properties of Mn_2AlB_2 under high pressure

Yi-Xian Wang(王乙先), Zhe Yuan(袁喆), Wu-Na Xie(谢武娜), Yi-Yang Qiu(邱一洋), and Zhao-Qi Wang(王朝棋)
Chin. Phys. B, 2026, 35 (**7**): 076105. DOI: 10.1088/1674-1056/ae3134

High-pressure synthesis, crystal structure, and electronic properties of $Ba_9Zr_{2.79}Te_{15}$

Runteng Chen(陈润滕), Guodong Wang(王国东), Zhe Wang(王哲), Wenmin Li(李文敏), Jianfa Zhao(赵建发), Zheng Deng(邓正), Heng Wang(王恒), Xiancheng Wang(望贤成), Jun Zhang(张俊), and Changqing Jin(靳常青)
Chin. Phys. B, 2026, 35 (**6**): 066101. DOI: 10.1088/1674-1056/ae521a

Structural stability and mechanical properties of TiB_6: A CALYPSO-guided exploration for superhard applications

Bo Sun(孙博), Yutong Zou(邹雨桐), Tao Wang(王淘), Yujia Wang(王雨佳), Jinyu Liu(刘金禹), Lili Gao(高丽丽), Meiguang Zhang(张美光), and Miao Zhang(张淼)
Chin. Phys. B, 2026, 35 (**5**): 056105. DOI: 10.1088/1674-1056/adfb59

Strain and ligand effect on the electronic structure of Ni-Fe and Ni-Cu alloys: Exploring charge redistribution from x-ray spectroscopies and the charge compensation model

Zeel Patel, Lu Yao, Zhiqiang Wang, Yun Mui Yiu, Tsun-Kong Sham, Sarah Purdy, Jianfeng Zhu, and Sammynaiken Ramaswami
Chin. Phys. B, 2026, 35 (**5**): 056101. DOI: 10.1088/1674-1056/ae3691

Physical properties of Cr_2S_3 at high pressure

Lun Xiong(熊伦), Mingquan Jiang(江明全), Jinxia Zhu(竹锦霞), Lin Xia(夏林), Hao Wang(王毫), Shenghan Zhang(张升瀚), Pengfei Tang(汤鹏飞), Zhiqiang Chen(陈志强), Sheng Jiang(蒋升), and Hongliang Dong(董洪亮)
Chin. Phys. B, 2026, 35 (**3**): 036103. DOI: 10.1088/1674-1056/ae1cb3

Pressure tunable magnetic skyrmion phase in $Co_8Zn_8Mn_4$ single crystals

Zhun Li(李准)[1,2,3,4,†], Xinrun Mi(米薪润)[1,†], Xinmin Wang(王欣敏)[2,3,4], Jian Lyu(吕坚)[2,3,4], Na Su(苏娜)[1], Aifeng Wang(王爱峰)[1], Yisheng Chai(柴一晟)[1], Bao Yuan(袁宝)[2,3,4], Wanju Luo(罗万居)[2,3,4], Hui Cheng(程辉)[2,3,4], Jianxiang Gao(高健翔)[5], Hongliang Wang(王洪亮)[5], Lijie Hao(郝丽杰)[5], Mingquan He(何明全)[1,‡], Junying Shen(沈俊英)[2,3,4,§], Young Sun(孙阳)[1,¶], and Xin Tong(童欣)[2,3,4,‖]

[1] *College of Physics & Center of Quantum Materials and Devices, Chongqing University, Chongqing* 401331, *China*
[2] *Institute of High Energy Physics, Chinese Academy of Sciences (CAS), Beijing* 100049, *China*
[3] *Spallation Neutron Source Science Center, Dongguan* 523803, *China*
[4] *Guangdong Provincial Key Laboratory of Extreme Conditions, Dongguan* 523803, *China*
[5] *Neutron Scattering Laboratory, Department of Nuclear Physics, China Institute of Atomic Energy, Beijing* 102413, *China*

(Received 1 August 2025; revised manuscript received 10 October 2025; accepted manuscript online 16 October 2025)

In a magnetic skyrmion phase, magnetic moments form vortex-like topological textures which are of both fundamental and industrial interest. In β-Mn-type Co–Zn–Mn alloys, chiral magnetic skyrmions emerge above room temperature, providing a unique system for studying the skyrmion physics and exploring spintronics applications. However, the magnetic skyrmion phase is typically confined in a narrow and limited temperature (T) and magnetic field (H) range. Here, we demonstrate that quasihydrostatic pressure can expand the skyrmion phase in the T–H phase diagram of single-crystalline $Co_8Zn_8Mn_4$. At ambient pressure, signatures of skyrmions are seen within $T \sim 302$ K–308 K and $H \sim 50$ Oe–100 Oe (1 Oe = 79.5775 A·m^{-1}). Applying a moderate pressure of 6 kbar (1 bar = 10^5 Pa) extends this range to $T \sim 300$ K–310 K and $H \sim 50$ Oe–150 Oe. However, further escalation of pressure to 10 kbar results in a slight contraction of the skyrmion phase. These findings underscore the sensitivity of the skyrmion phase in $Co_8Zn_8Mn_4$ to external pressures, and hint at the potential of strain engineering, particularly in β-Mn-type Co–Zn–Mn thin films, as a promising avenue to customize the skyrmion phase.

Keywords: magnetic skyrmions, Dzyaloshinskii–Moriya (DM) interaction, CoZnMn, pressure

PACS: 61.50.Ks, 75.30.Kz, 75.75.–c, 75.80.+q

DOI: 10.1088/1674-1056/ae13ed **CSTR:** 32038.14.CPB.ae13ed

1. Introduction

Magnetic skyrmions, distinguished by their unique vortex-like spin configurations carrying integer topological charges, have become a forefront in the study of condensed matter physics and material science.[1–3] The nontrivial spin textures of skyrmions are fascinating both from a fundamental physics perspective and for their potential technological applications. Fundamentally, magnetic skyrmions can arise through diverse mechanisms, such as the interplay between ferromagnetic exchange, Dzyaloshinskii–Moriya (DM), Ruderman–Kittel–Kasuya–Yosida (RKKY), and magnetic dipolar interactions.[2–7] From a technological standpoint, skyrmions stand out for their emergent electromagnetic properties and the ability to be manipulated with low current densities, making them highly efficient for advanced spintronics applications.[8–10]

In bulk materials, magnetic skyrmions are commonly observed in chiral magnets, such as metallic B20 compounds (MnSi, $Fe_{1-x}Co_xSi$, FeGe) and insulating Cu_2OSeO_3.[2,3,11,12] In these non-centrosymmetric compounds, a helimagnetic state is typically formed below a certain magnetic Curie temperature (T_c) due to the competition between DM and ferromagnetic exchange interactions. In the presence of magnetic fields, a skyrmion crystal (SkX) phase emerges in the vicinity of T_c. However, the T_c values of the aforementioned chiral magnets lie below room temperature, limiting the applications of skyrmions. Interestingly, this limitation is overcome in another type of chiral magnets, *i.e.*, the β-Mn-type $Co_xZn_yMn_z$ ($x+y+z=20$) alloys.[13] The Curie temperatures of $Co_xZn_yMn_z$ depend strongly on compositions and $T_c > 300$ K can be realized when $z \leq 4$.[13] Above room temperature, skyrmion lattices have been observed in a series of $Co_xZn_yMn_z$.[13–18] Like the B20 compounds, the SkX phase in $Co_xZn_yMn_z$ is typically confined in a narrow temperature

†These authors contributed equally to this work.
‡Corresponding author. E-mail: mingquan.he@cqu.edu.cn
§Corresponding author. E-mail: shenjy@ihep.ac.cn
¶Corresponding author. E-mail: youngsun@cqu.edu.cn
‖Corresponding author. E-mail: tongx@ihep.ac.cn

© 2026 Chinese Physical Society and IOP Publishing Ltd. All rights, including for text and data mining, AI training, and similar technologies, are reserved.

(T) and magnetic field (H) region near T_c, as a result of the interplay between long-range magnetic interactions and thermal fluctuations.[13–18] A goal in the study of skyrmions in bulk chiral magnets is to expand the temperature and magnetic field window which supports the SkX phase.

It has been found that long-lived metastable skyrmions in $Co_xZn_yMn_z$ can survive in a wide temperature range well below T_c, achieved via the assistance of magnetic frustrations, disorders, or field-trained cooling.[14,18–20] In addition, pressure or strain is another effective tuning parameter in manipulating crystal structure, magnetic interactions, and magnetic phases. It has been theoretically suggested that uniaxial anisotropy induced by uniaxial strain can stabilize the skyrmion phase of MnSi, FeGe, and $Fe_{1-x}Co_xSi$ in a broad temperature and magnetic field range.[21] Indeed, as found experimentally, the skyrmion phase in MnSi can be easily controlled by quasihydrostatic pressure,[22] uniaxial pressure,[23] and uniaxial stress.[24] Applying a moderate strain[25] or quasihydrostatic pressure[26] to Cu_2OSeO_3 significantly enlarges the skyrmion pocket spanned in the T–H phase diagram. Pressure control of the skyrmion phase in $Co_xZn_yMn_z$ alloys is, however, yet to be investigated.

In this article, we study the effects of quasihydrostatic pressure on the skyrmion phase in single crystals of $Co_8Zn_8Mn_4$. At ambient pressure, the skyrmion phase is found to exist within about 5 K just below T_c. This temperature window is almost doubled under a moderate pressure of 6 kbar. The magnetic field range of the skyrmion pocket is also enlarged under pressure. Pressure is thus a sensitive tuning knob in controlling the skyrmion phase in $Co_8Zn_8Mn_4$.

2. Experimental methods

Single crystals of $Co_8Zn_8Mn_4$ were grown using the Bridgman method.[27] A precursor $Co_xZn_yMn_z$ ($x+y+z=20$) was first synthesized via a solid-state reaction. Pure Co (99.99%), Zn (99.99%), and Mn (99.99%) grains were mixed in a quartz tube, which was then sealed in a vacuum environment. The mixture was heated to 1000 °C and kept at this temperature for 24 h. It was then slowly cooled down to 925 °C at a rate of 1 °C/h, followed by water quenching. Then the product was ground thoroughly in an agate mortar, and the precursor complexes of $Co_8Zn_8Mn_4$ were obtained. Finally, we used these precursor complexes according to the method described in Ref. [28] to grow single crystals of $Co_8Zn_8Mn_4$.

The composition of the as-prepared single crystals was determined by energy-dispersive x-ray spectroscopy (EDX). Both powder x-ray diffraction and single-crystal x-ray diffraction (XRD) measurements were performed on a Malvern Panalytical EMPYREAN SERIES 3 diffractometer, and the latter was carried out on a large piece of $Co_8Zn_8Mn_4$ single crystal (4.20 mm ×2.5 mm×0.25 mm). Single-crystal neutron diffraction experiments were carried out on a four-circle neutron diffractometer in the Chinese Advanced Research Reactor. An incident beam with a wavelength of 0.9085 Å was used, selected by a vertically focusing Cu (220) monochromator crystal.

DC magnetization and ac magnetic susceptibility of $Co_8Zn_8Mn_4$ samples were measured in a superconducting quantum interference device magnetometer (MPMS-3, Quantum Design). For the ac magnetic susceptibility experiments, an excitation amplitude of 1 Oe and a frequency of 10 Hz were used. DC magnetization under pressure was measured in the magnetic properties measurement system (MPMS-3, Quantum Design) using a miniature piston pressure cell with Daphne 7373 as the pressure transmitting medium, and Sn was loaded into a Teflon capsule along with the sample. The applied pressure at low temperatures was determined by monitoring the pressure-dependent superconducting transition temperature of Sn. The corresponding pressure at room temperature was estimated by adding a constant of 1.6 kbar to the pressure obtained at low temperatures, as the pressure difference for the pressure-transmitting medium Daphne 7373 between 300 K and 4.2 K is consistently between 1.5 kbar and 1.7 kbar.[29] We note that although Daphne 7373 remains liquid up to about 30 kbar at room temperature,[30] pressure inhomogeneity inevitably exists (approximately 5% at 13.4 kbar and 300 K).[31] Therefore, only quasihydrostatic conditions were achieved in the temperature and pressure ranges studied here. For all field-dependent measurements, the external magnetic field was consistently applied along the [110] crystalline direction on the same crystal, with the field swept upwards.

The magnetostriction coefficient of a $Co_8Zn_8Mn_4$ single crystal was measured using a composite magnetoelectric (ME) method.[32,33] The $Co_8Zn_8Mn_4$ sample was mechanically bonded to a piezoelectric PMN-PT [$0.7Pb(Mg_{1/3}Nb_{2/3})O_3$–$0.3PbTiO_3$] transducer using silver epoxy. The PMN-PT is a [001]-cut thin plate with a thickness of 0.2 mm. In a magnetic field, the magnetostrictive length deformation of $Co_8Zn_8Mn_4$ is transferred to PMN-PT, generating an electronic voltage via the piezoelectric effect. The recorded ME voltage coefficient α_{ME} can be formulated as

$$\alpha_{ME} = k\frac{dE}{d\lambda}\frac{d\lambda}{dH}, \tag{1}$$

where $0 < k < 1$ is a strain transmission constant between the mechanically bonded $Co_8Zn_8Mn_4$ sample and PMN-PT, λ is the magnetostriction, $d\lambda/dH$ is the magnetostriction coefficient, and $dE/d\lambda$ is the piezoelectric coefficient. During the experiments, a small ac magnetic field was superimposed on a DC magnetic field, giving rise to an ac ME signal $\alpha_{ME} = \alpha_x + i\alpha_y$ [see Fig. 3]. The ac magnetic field was generated by a homemade Helmholtz coil. An excitation amplitude

of 1 Oe and a frequency of 422 Hz were used for the ac magnetostriction measurements. The ac ME data were collected using the lock-in technique.

3. Results and discussion

β-Mn-type $Co_xZn_yMn_z$ ($x+y+z=20$) alloys crystallize in a cubic structure belonging to the chiral space group $P4_132$ [see Fig. 1(b) inset] or $P4_332$.[27,34] These two types of space group host different chiralities and can be interchanged by a mirror operation. There are two different Wyckoff sites (8*c* and 12*d*) occupied by 20 atoms in each unit cell. The Co atoms are coordinated at the 8*c* sites, and the Zn/Mn atoms are located at the 12*d* sites.[13–18,35] Figure 1(a) shows the x-ray diffraction data obtained on $Co_8Zn_8Mn_4$ powders. The observed data can be well described by the β-Mn cubic chiral structure. The refined lattice constants give $a=b=c=6.3617$ Å, agreeing well with previous reports.[19] Detailed structure parameters are listed in Table 1. It is seen that minor Mn atoms also enter the 8*c* sites, which typically happens in $Co_xZn_yMn_z$ compounds with $z \geq 4$.[16] In Fig. 1(b), x-ray diffraction patterns captured from a typical $Co_8Zn_8Mn_4$ single crystal are shown. Two sharp peaks can be nicely indexed by (2,2,1) and (4,4,2), respectively. The quality of the $Co_8Zn_8Mn_4$ sample is further checked by single-crystal neutron diffraction, as displayed in Figs. 1(c)–1(f). Rocking curves near four typical Bragg peaks are nicely resolved and both peaks show a very narrow full width at half maximum (FWHM) about 0.16 degrees, in good agreement with the reported data.[19] All these results point to the high quality of the single crystal.

Table 1. The structure parameters of $Co_8Zn_8Mn_4$ extracted from powder x-ray diffraction data measured at room temperature. The space group is $P4_132$, $a=b=c=6.3788$ Å, $R_p=133.0$, $R_{wp}=45.0$, $R_e=35.5$, GOF = 21.463.

Atom	Wyckoff	*x*	*y*	*z*	Biso.	Occ.
Co(1)	8*c*	0.06618	0.06618	0.06618	0.43207	0.3333
Zn(1)	8*c*	0.06618	0.06618	0.06618	0.43207	0
Mn(1)	8*c*	0.06618	0.06618	0.06618	0.43207	0
Co(2)	12*d*	0.125	0.20106	0.45106	0.96504	0
Zn(2)	12*d*	0.125	0.20106	0.45106	0.96504	0.33333
Mn(2)	12*d*	0.125	0.20106	0.45106	0.96504	0.16666

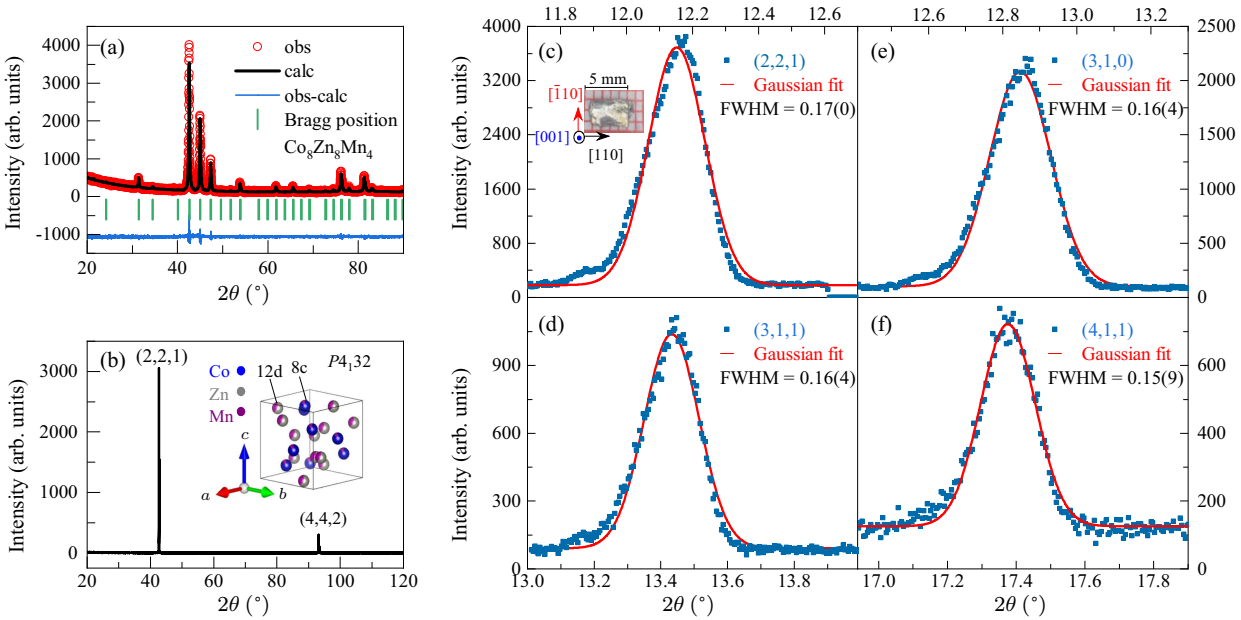


Fig. 1. (a) Powder x-ray diffraction pattern of the as-prepared $Co_8Zn_8Mn_4$ samples. Red circles are experimental observations. The black line is calculated diffraction data. The differences between experimental results and calculated data are presented in the blue curve. Bragg peaks are marked out by green vertical lines. (b) Single-crystal x-ray diffraction results of a $Co_8Zn_8Mn_4$ sample. The inset in panel (b) shows the crystal structure of β-Mn-type $Co_xZn_yMn_z$ alloys. (c)–(f) Rocking curves near four Bragg peaks measured using single-crystal neutron diffraction. The full width at half maximum (FWHM) of each peak is estimated by fitting the corresponding peak to a Gaussian profile (red line). A photograph of a typical $Co_8Zn_8Mn_4$ single crystal is shown in the inset in panel (c).

Figure 2 shows DC magnetization data of a $Co_8Zn_8Mn_4$ single crystal. In a weak magnetic field ($H=20$ Oe), a clear ferromagnetic-like transition is seen at $T_c=309$ K in the temperature-dependent magnetization experiments [Fig. 2(a)]. The transition temperature is slightly higher than that ($T_c \sim 300$ K) reported in other studies.[13,18,19] This minor difference is likely caused by slight variations in compositions, since T_c is sensitive to the Mn concentration.[13,14,16,18] In zero field and below T_c, $Co_8Zn_8Mn_4$ enters a helical magnetic state with a periodicity of $\lambda \sim 125$ nm.[13,19] Below T_c, the temperature

dependence of magnetization deviates from a typical ferromagnet, especially at low temperatures. Below about 150 K, the magnetization decreases gradually with cooling, both in zero-field-cooled (ZFC) and field-cooled (FC) measurements. In addition, a sharp drop is seen in ZFC data below $T_g \sim 20$ K. The transition occurring at T_g is caused by a re-entrant spin-glass transition, which is commonly observed in $Co_xZn_yMn_z$ for $3 \leq z \leq 19$.[14,16,18] It has been suggested that Co moments order magnetically below T_c, while Mn moments remain fluctuating with cooling until T_g, below which a spin-glass state is formed.[16,17] In Fig. 2(b), the magnetization near T_c is plotted as a function of magnetic field ($H \parallel [110]$). Below T_c, the magnetization rises rapidly with increasing magnetic field and becomes saturated above about 150 Oe. In the saturated region, magnetic moments are ferromagnetically polarized though the magnetization further increases slightly in higher fields. Slightly above T_c, nonlinear $M(H)$ curves are also seen, suggesting sizable spin fluctuations. As shown in Fig. 2(a), the onset of the spin–spin correlation starts already below 330 K. And linear $M(H)$ is almost restored at 320 K [Fig. 2(b)]. Note that signatures of skyrmions are masked by the rapid variations of magnetization in small magnetic fields. Transitions between different magnetic phases are seen more clearly in the derivative form dM/dH, as shown later in Fig. 4.

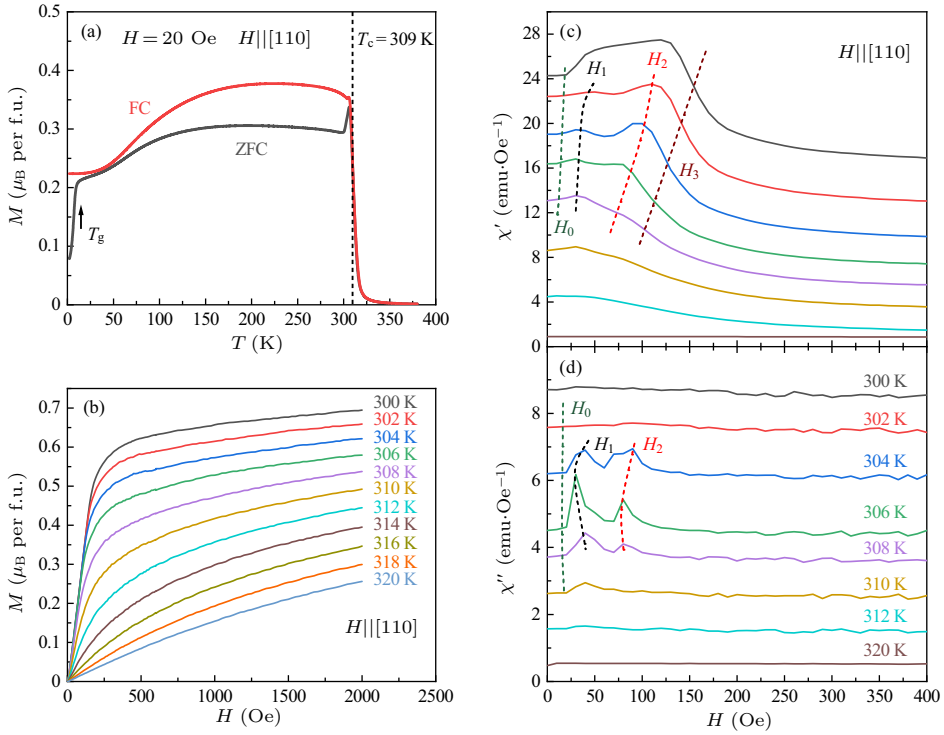


Fig. 2. (a) Temperature dependence of magnetization measured in a small dc magnetic field ($H = 20$ Oe) applied along the [110] direction. Both zero-field-cooled (ZFC) and field-cooled (FC) data reveals a ferromagnetic-like transition at $T_c = 309$ K. A re-entrant spin-glass transition occurs at $T_g \sim 20$ K as seen in the ZFC data. (b) Magnetization as a function of magnetic field recorded at selected temperatures near T_c. (c) and (d) Real (χ') and imaginary χ'' parts of the ac susceptibility, respectively. Curves have been shifted vertically for clarity. Green (H_0), black (H_1), red (H_2), and dark red ((H_3)) lines mark the field boundaries between different magnetic phases. The skyrmion phase only exists between H_1 and H_2.

To access the skyrmion phase, we present ac susceptibility $\chi = \chi' + i\chi''$ in Figs. 2(c) and 2(d). Between 302 K and 306 K, a clear dip is seen around 50 Oe in both the real (χ') and imaginary (χ'') parts of ac susceptibility. This dip structure, commonly observed in skyrmion hosts B20 compounds and Cu_2OSeO_3,[12,36,37] is a characteristic thermodynamic signature of skyrmion lattice in $Co_8Zn_8Mn_4$.[13] The magnetic fields H_1 and H_2 mark the lower and upper boundaries of the skyrmion pocket. As found by earlier reports, the skyrmion phase is sandwiched by conical states.[13,14,16,18] The H_1 and H_2 are thus critical fields differentiating the skyrmion and conical phases. The transition between the zero-field helimagnetic and conical states happens at a lower field H_0, below which χ' depends weakly on H. In the vicinity of a higher magnetic field H_3, χ' drops rapidly and a polarized ferromagnetic state is achieved above H_3.

In addition to the ac magnetic susceptibility, the ac ME coefficient, which is proportional to magnetostriction, is another thermodynamic probe for sensing the skyrmion phase.[32,33,38,39] Distinct magnetostrictive features have been observed in the skyrmion phase of MnSi[32,39] and $Co_7Zn_8Mn_5$.[33] Figures 3(a) and 3(b) show the ac ME coefficient results of $Co_8Zn_8Mn_4$. At temperatures above T_c, both the real (α_x) and imaginary (α_y) components of the ac ME coefficient vary smoothly with magnetic field. At 308 K, just below T_c, a kink in α_x and a peak in α_y are observed at H_0, indicating the transition from the helical to conical phase. At a slightly higher magnetic field H_1, a broad maximum in α_x and

a clear dip in α_y mark the transition between the conical and skyrmion phases. Upon further cooling, these features at H_0 and H_1 become more pronounced [see Fig. 3(d)]. Near H_2, α_x rises steeply while α_y becomes nearly field-independent, indicating the transition from the conical to ferromagnetic state, visualized as a broad peak in α_x near H_3. Below 302 K, signatures of the skyrmion phase gradually fade, consistent with the ac susceptibility data. In Figs. 3(c) and 3(d), the results obtained by dc magnetization, ac susceptibility, and ac ME coefficient are directly compared. It is seen that the skyrmion phase is consistently observed in all three thermodynamic probes. The critical magnetic fields associated with various magnetic transitions are also nicely identified.

The magnetostriction coefficient $\mathrm{d}\lambda(H)/\mathrm{d}H$ is directly proportional to the product of the magnetization $\langle S_k^z \rangle$ and the spin-spin correlation $\langle \boldsymbol{S}_i \cdot \boldsymbol{S}_j \rangle$ via the magnetoelastic coupling $D(i,j)$: $\mathrm{d}\lambda(H)/\mathrm{d}H \sim \sum_{k\langle i,j \rangle} D(i,j) \langle S_k^z \boldsymbol{S}_i \cdot \boldsymbol{S}_j \rangle$, making it highly sensitive to spin fluctuations.[40,41] As shown in Fig. 3(e), α_x is vanishingly small well above T_c in the paramagnetic phase. Upon cooling below 330 K, α_x rises rapidly, peaking at $T^* \sim 312$ K due to the development of spin fluctuations. In zero magnetic field, α_x also diverges as it approaches T^*, though with significantly smaller amplitudes compared to those in non-zero magnetic fields. The peak in α_x at T^* signifies the crossover between the paramagnetic state and the disordered fluctuating phase, characterized by short-range correlations, as found in MnSi.[32,42] Below T^*, the establishment of short-range correlations suppresses spin fluctuations, leading to a rapid decrease in α_x. Below T_c, the onset of long-range order further suppresses spin fluctuations and α_x. It is noteworthy that α_x changes slope at T_c [see the inset in Fig. 3(e)]. A dip appears in α_x below T_c in small magnetic fields, indicating transitions between different ordered states. Note that the disordered fluctuating region between T_c and T^* is not resolved in magnetization measurements [see Fig. 2(a)]. The superior sensitivity to spin fluctuations makes the magnetostriction coefficient a prominent probe for tracking complex magnetic transitions.

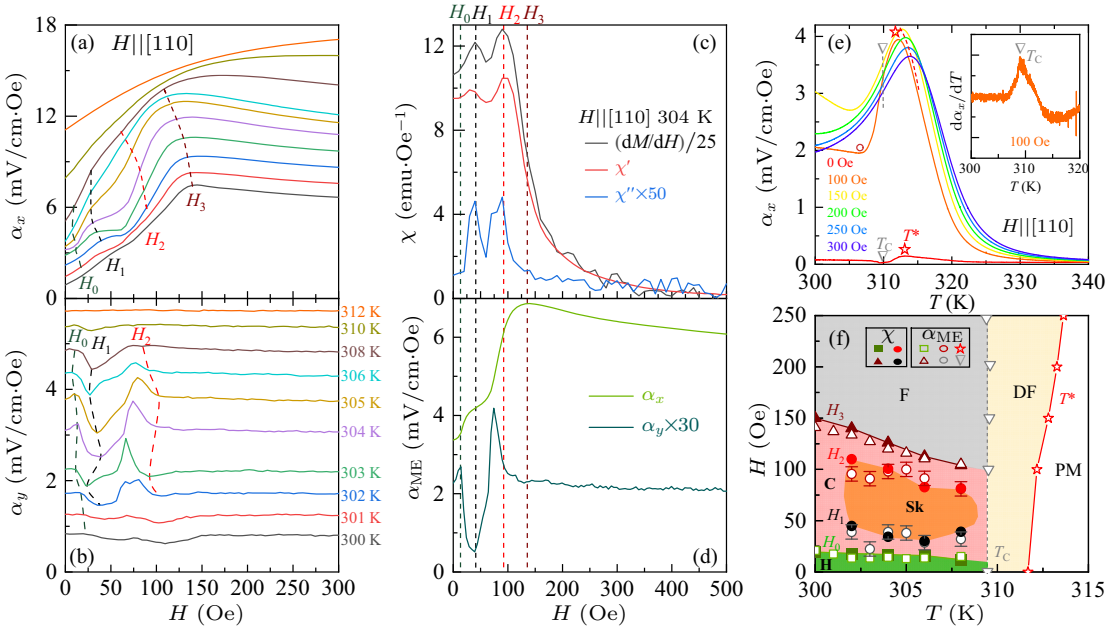


Fig. 3. (a) and (b) Real (α_x) and imaginary α_y parts of the ac ME coefficient measured near T_c. Curves have been shifted vertically for clarity. (c) and (d) Comparison of dc magnetization, ac susceptibility and ac ME coefficient recorded at 304 K. The χ'', α_y, and $\mathrm{d}M/\mathrm{d}H$ lines are multiplied by 50, 30, and 1/25 for better visualization. (e) Temperature-dependent ac ME coefficient measured near T_c. The inset in panel (e) shows the temperature derivative of α_x recorded in 100 Oe. (f) T–H phase diagram $Co_8Zn_8Mn_4$ obtained using ac susceptibility (solid symbols) and ac ME coefficient (open symbols) results. In addition to the commonly reported helical (H), conical (C), skyrmion (Sk), and polarized ferromagnetic (F) ordered states, a disordered fluctuating (DF) region is seen between the magnetic ordered and paramagnetic (PM) phases.

Based on the ac susceptibility and ac ME data, the phase diagram of $Co_8Zn_8Mn_4$ single crystals measured at ambient pressure is mapped out in Fig. 3(e). Similar phase diagrams are commonly seen in $Co_xZn_yMn_z$ alloys.[13,14,16,18] In zero magnetic field, a helical (H) magnetic state is formed below $T_c = 309$ K. In the magnetically ordered state just below T_c, applying a magnetic field between H_1 and H_2 drives the system into a skyrmion phase. Clearly, the skyrmion (Sk) pocket is confined in a narrow region sandwiched by a conical (C) phase in the T–H phase diagram. Moderate magnetic fields above H_3 drive the system into a polarized ferromagnetic (FM) state. In addition, a disordered fluctuating (DF) region is found between the magnetic ordered state and paramagnetic (PM) state.

Now we explore the effects of quasihydrostatic pressure on the skyrmion phase of $Co_8Zn_8Mn_4$. DC magnetization measured under different pressures is shown in Figs. 4(a)–4(c). At ambient pressure (P_0), the skyrmion phase is manifested as a dip in $\mathrm{d}M/\mathrm{d}H$ within $T \sim 302$ K–306 K and $H \sim 50$ Oe–100 Oe, as also found in ac susceptibility. By applying a mod-

erate pressure of $P_1 = 6.1$ kbar, as presented in Fig. 4(b), the dip feature in $\mathrm{d}M/\mathrm{d}H$ appears already at 310 K and persists down to 300 K. The absolute height of the dip structure is also enhanced compared to that in P_0. Moreover, both the lower (H_1) and upper (H_2) magnetic field boundaries of the skyrmion phase are clearly increased. This trend persists to a higher pressure $P_2 = 9.6$ kbar as shown in Fig. 4(c). Note that compared with P_1, the upper temperature limit in P_2 is slightly reduced back to 308 K. Figure 4(d) summarizes the phase diagram occupied by the skyrmion pocket under different pressures. Clearly, the area covered by the skyrmion phase in the T–H phase diagram is significantly enlarged under pressure. Under the pressure of P_1, the absolute size of the skyrmion pocket is more than twice that at ambient pressure (P_0). It has been shown that the skyrmion phase of $Co_8Zn_8Mn_4$ forms a triangular equilibrium lattice at ambient pressure.[13,18,19] Our observation rules out possibilities of other topological spin textures such as magnetic meron or magnetic bubble. Magnetic meron is considered to locate between helical phase and skyrmion phase,[43] thus a pressure-induced magnetic meron would present at lower field below H_1. Magnetic bubbles hold magnetic domains and own different energy scales than skyrmion,[44] thus, a pressure-induced bubble phase would monotonically evolve with increasing pressure. Furthermore, the spatial organization of skyrmions formed under pressure remains to be explored.

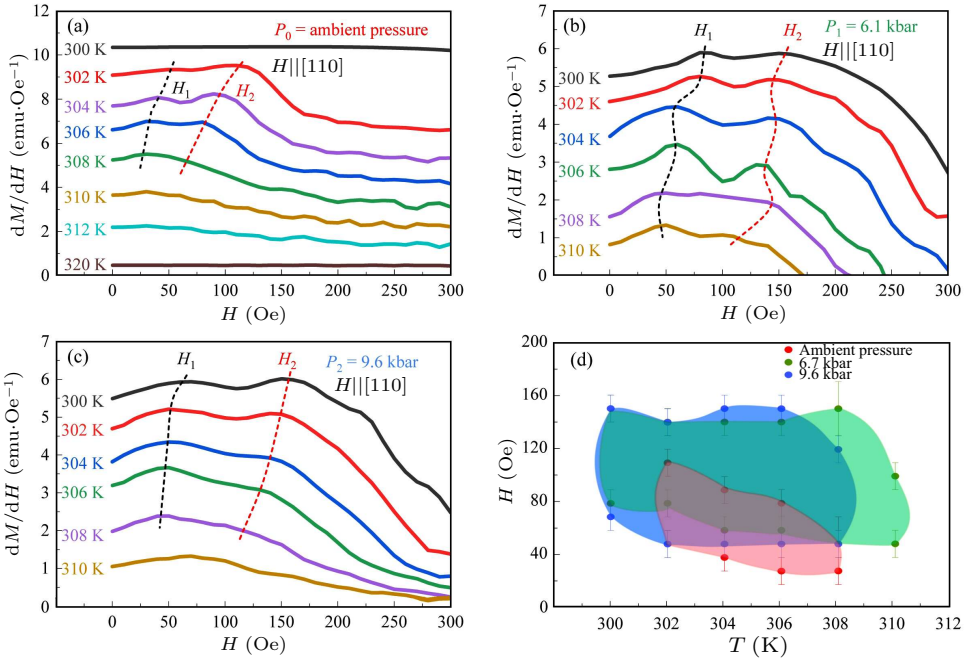


Fig. 4. (a)–(c) The dc magnetization of a $Co_8Zn_8Mn_4$ single crystal measured under different pressures. Curves have been shifted vertically for clarity. (d) Comparison of the skyrmion phase captured under different pressures. The skyrmion pocket is clearly enlarged under pressure.

Pressure-tuned expansion of the skyrmion phase has been previously observed in bulk MnSi,[22–24] Cu_2OSeO_3.[25,26] Since the skyrmion phase emerges near T_c, the free energy of the system can thus be described by the Ginzburg–Landau approach:[22,26] $F[\boldsymbol{M}] = A\boldsymbol{M}^2 + J(\nabla \boldsymbol{M})^2 + D\boldsymbol{M} \cdot (\nabla \times \boldsymbol{M}) + (U+K)\boldsymbol{M}^4 - \mu_0 \boldsymbol{H} \cdot \boldsymbol{M}$, where the magnetization M is the order parameter, A is a temperature-dependent constant controlling T_c, J represents the ferromagnetic exchange interactions, D is the DM interaction, U describes the mode-mode interactions, and K accounts for magnetic anisotropy. Applying pressure tunes the parameters J, D, and K, which in turn manipulates the size of the skyrmion phase. Although relatively small compared to the exchange and DM interactions, magnetic anisotropy plays an essential role in stabilizing the skyrmion phase in Cu_2OSeO_3,[45–47] β-Mn-type $Co_xZn_yMn_z$ compounds,[19,48,49] and multilayer structures.[50–52] Based on the Ginzburg–Landau analysis, Levati'c *et al.* demonstrated that the skyrmion phase is most sensitive to variations in K among the pressure-tuned parameters.[26] A moderate increase in K significantly enlarges the skyrmion phase in Cu_2OSeO_3,[26] while modulation of the DM interaction often leads to large deformations of the skyrmion lattice, as observed in FeGe thin plates.[53] Consequently, it is now widely accepted that pressure- or strain-induced changes in magnetic anisotropy, though small, play a crucial role in expanding the skyrmion phase.[21–26] In the case of $Co_8Zn_8Mn_4$, pressure-tuned magnetic anisotropy is likely the key factor responsible for the expansion of the skyrmion phase under moderate pressure. In addition, magnetic fluctuations also play important roles in stabilizing the skyrmion phase, as found in $Co_7Zn_7Mn_6$.[20] Under 6.1 kbar, the skyrmion phase of $Co_8Zn_8Mn_4$ extends up to about 310 K, slightly above the T_c at ambient pressure. Stabilization of short-range correlations in the DF region under pressure may also contribute to the

pressure-induced extension of the skyrmion pocket.

Note that pressure-induced structural changes can significantly enhance the skyrmion phase, as observed in Cu_2OSeO_3 at high pressures of 420 kbar.[54] However, at moderate pressures, such as those in our study (below 10 kbar), significant pressure-induced structural changes are not expected. Nevertheless, pressure inhomogeneities and local strains may still occur, potentially leading to enhanced stability of the skyrmion phase.[22,55] The effects of pressure inhomogeneities or local strain on the skyrmion phase can become significant, particularly when the pressure-transmitting medium is in its solid phase.[55] For example, Levati'c *et al.* reported pronounced pressure-induced enlargement of the skyrmion phase in Cu_2OSeO_3 using the pressure-transmitting medium Daphne 7373 in its solid state.[26] In contrast, negligible pressure-tuning effects on the skyrmion phase in Cu_2OSeO_3 were observed by Crisanti *et al.* using liquid helium as the pressure-transmitting medium.[55] Even in the liquid phase of helium, applied pressure imposed directional stress, slightly modulating the domain population of Cu_2OSeO_3.[55]

In our study, using Daphne 7373 as the pressure-transmitting medium, pressure inhomogeneity of approximately 5% may arise at 13.4 kbar,[31] well below the solidification pressure (about 30 kbar[30]). After solidification, pressure inhomogeneities can increase up to 30%.[31] Although the effects of pressure inhomogeneities on the skyrmion phase of $Co_8Zn_8Mn_4$ cannot be completely ruled out, we believe they play a subdominant role for the following reasons: (i) Since Daphne 7373 remains in its liquid phase within the temperature and pressure range studied here, moderate pressure inhomogeneities of a few percent are unlikely to significantly impact the skyrmion pocket, as also found in Cu_2OSeO_3;[52] (ii) Higher pressure inhomogeneity would be expected at 9.6 kbar compared to 6.1 kbar, yet the skyrmion phase shrinks in the former case. The effect of pressure inhomogeneity or directional strain on $Co_8Zn_8Mn_4$ could lead to slight differences in stress on transverse and longitudinal directions, similar to the study of MnSi,[24] or weaker modulation on D relating to the complex near-E_F electronic bands of $Co_8Zn_8Mn_4$ compared to the modulation by strain on FeGe,[51] thus resulting in a weak shrinkage of its skyrmion pocket. On the other hand, if the remarkable enlargement of the skyrmion pocket in $Co_8Zn_8Mn_4$ is indeed induced by such moderate pressure inhomogeneities or directional strain, it would be promising to explore strain-tuning of the skyrmion phase. This opens up exciting possibilities for developing skyrmion-based devices using $Co_8Zn_8Mn_4$ thin films. We also note that magnetic frustrations or disorders can induce metastable skyrmion phases in $Co_xZn_yMn_z$.[14,18] While magnetic frustrations or disorders are mostly arising from Mn atoms located on the 12d sites, giving rise to metastable skyrmion phases at low temperatures. The pressure-expanded skyrmion pocket near T_c found in $Co_8Zn_8Mn_4$ is thus unlikely caused by magnetic frustrations or disorders.

4. Conclusions

In summary, we have studied the evolution of the skyrmion phase in $Co_8Zn_8Mn_4$ under quasihydrostatic pressure. It is found that the size of the skyrmion pocket on the T–H phase diagram is considerably enlarged under a moderate pressure of about 10 kbar. Although pressure inhomogeneities may exist, the enhanced stability of the skyrmion phase is likely caused by pressure-driven enhancement of magnetic anisotropy. It would be interesting to further manipulate the skyrmion phase using strain engineering on $Co_xZn_yMn_z$ thin films or by even higher pressure or doping to change the crystal structure of bulk $Co_xZn_yMn_z$ compounds.

Acknowledgements

Project supported by the National Natural Science Foundation of China (Grant Nos. 12104254 and 12227806), the Joint Funds of the National Natural Science Foundation of China (Grant No. U2430209), Chinesisch–Deutsche Mobilitätsprogamm of Chinesisch–Deutsche Zentrum für Wissenschaftsförderung (Grant No. M-0496), Guangdong Innovative and Entrepreneurial Research Team Program (Grant No. 2021ZT09C539), the Open Fund of the China Spallation Neutron Source Songshan Lake Science City (Grant No. KFKT2023B07), the Fundamental and Applied Fundamental Research Grant of Guangdong Province, China (Grant No. 2021B1515120015), the Natural Science Funds for Distinguished Young Scholar of Guangdong Province, China (Grant No. 2021B1515020101), the National Science Fund for Distinguished Young Scholars (Grant No. 12425512), and the National Key Research and Development Program of China (Grant No. 2023YFA1610000).

References

[1] Bogdanov A N and Yablonskii D 1989 *Sov. Phys. JETP* **68** 101
[2] Mühlbauer S, Binz B, Jonietz F, Pfleiderer C, Rosch A, Neubauer A, Georgii R and Böni P 2009 *Science* **323** 915
[3] Yu X Z, Onose Y, Kanazawa N, Park J H, Han J H, Matsui Y, Nagaosa N and Tokura Y 2009 *Nature* **465** 901
[4] Yu X Z, Tokunaga Y, Kaneko Y, Zhang W Z, Kimoto K, Matsui Y, Taguchi Y and Tokura Y 2014 *Nat. Commun.* **5** 3198
[5] Wang W, Zhang Y, Xu G Z, Peng L, Ding B, Wang Y, Hou Z, Zhang X, Li X, Liu E, Wang S, Cai J, Wang F, Li J, Hu F, Wu G, Shen B and Zhang X X 2016 *Adv. Mater.* **28** 6887
[6] Kurumaji T, Nakajima T, Hirschberge M, Kikkawa A, Yamasaki Y, Sagayama H, Nakao H, Taguchi Y, Arima T and Tokura Y 2019 *Science* **365** 914
[7] Hirschberger M, Nakajima T, Gao S, Peng L, Kikkawa A, Kurumaji T, Kriener M, Yamasaki Y, Sagayama H, Nakao H, Ohishi K, Kakurai K, Taguchi Y, Yu X, Arima T and Tokura Y 2019 *Nat. Commun.* **10** 5831
[8] Jonietz F, Mühlbauer S, Pfleiderer C, Neubauer A, Münzer W, Bauer A, Adams T, Georgii R, Böni P, Duine R A, Everschor K, Garst M and Rosch A 2010 *Science* **330** 1648

[9] Yu X Z, Kanazawa N, Zhang W Z, Nagai T, Hara T, Kimoto K, Matsui Y, Onose Y and Tokura Y 2012 *Nat. Commun.* **3** 988
[10] Iwasaki J, Mochizuki M and Nagaosa N 2010 *Nat. Nanotechnol.* **8** 742
[11] Yu X Z, Kanazawa N, Onose Y, Kimoto K, Zhang W Z, Ishiwata S, Matsui Y and Tokura Y 2011 *Nat. Mater.* **10** 106
[12] Seki S, Yu X Z, Ishiwata S and Tokura Y 2012 *Science* **336** 198
[13] Tokunaga Y, Yu X Z, White J S, Rønnow H M, Morikawa D, Taguchi Y and Tokura Y 2015 *Nat. Commun.* **6** 7638
[14] Karube K, White J S, Morikawa D, Dewhurst C D, Cubitt R, Kikkawa A, Yu X, Tokunaga Y, Arima T, Rønnow H M, Tokura Y and Taguchi Y 2018 *Sci. Adv.* **4** eaar7043
[15] Yu X Z, Koshibae W, Tokunaga Y, Shibata K, Taguchi Y, Nagaosa N and Tokura Y 2018 *Nature* **564** 95
[16] Nakajima T, Karube K, Ishikawa Y, Yonemura M, Reynolds N, White J S, Rønnow H M, Kikkawa A, Tokunaga Y, Taguchi Y, Tokura Y and Arima T 2019 *Phys. Rev. B* **100** 064407
[17] Bocarsly J D, Heikes C, Brown C M, Wilson S D and Seshadri R 2019 *Phys. Rev. Mater.* **3** 014402
[18] Karube K, White J S, Ukleev V, Dewhurst C D, Cubitt R, Kikkawa A, Tokunaga Y, Rønnow H M, Tokura Y and Taguchi Y 2020 *Phys. Rev. B* **102** 0644408
[19] Karube K, White J S, Reynolds N, Gavilano J L, Oike H, Kikkawa A, Kagawa F, Tokunaga Y, Rønnow H M, Tokura Y and Taguchi Y 2020 *Phys. Rev. B* **102** 0644408
[20] Ukleev V, Karube K, Derlet PM, Wang CN, Luetkens H, Morikawa D, Kikkawa A, Mangin-Thro L, Wildes AR, Yamasaki Y, Yokoyama Y, Yu L, Piamonteze C, Jaouen N, Tokunaga Y, Rønnow H M, Arima T, Tokura Y, Taguchi Y and White J S 2021 *npj Quantum Mater.* **6** 40
[21] Butenko A B, Leonov A A, Rößler U K and Bogdanov A N 2010 *Phys. Rev. B* **82** 052403
[22] Ritz R, Halder M, Franz C, Bauer A, Wagner M, Bamler R, Rosch A and Pfleiderer C 2013 *Phys. Rev. B* **87** 134424
[23] Chacon A, Bauer A, Adams T, Rucker F, Brandl G, Georgii R, Garst M and Pfleiderer C 2015 *Phys. Rev. Lett.* **115** 267202
[24] Nii Y, Nakajima T, Kikkawa A, Yamasaki Y, Ohishi K, Suzuki J, Taguchi Y, Arima T, Tokura Y and Iwasa Y 2015 *Nat. Commun.* **6** 8539
[25] Seki S, Okamura Y, Shibata K, Takagi R, Khanh N D, Kagawa F, Arima T and Tokura Y 2017 *Phys. Rev. B* **96** 220404
[26] Levatić I, Popčević P, Šurija V, Kruchkov A, Berger H, Magrez A, White JS, Rønnow Henrik M and Živković I 2016 *Sci. Rep.* **6** 21347
[27] Xie W, Thimmaiah S, Lamsal J, Liu J, Heitmann T W, Quirinale D, Goldman A I, Pecharsky V and Miller G J 2013 *Inorg. Chem.* **52** 9399
[28] Raquet B, Viret M, Sondergard E, Cespedes O and Mamy R 2002 *Phys. Rev. B* **66** 024433
[29] Murata, K, Yoshino H, Yadav H O, Honda Y and Shirakawa N 1997 *Rev. Sci. Instrum.* **68** 2490
[30] Keiichi Y, Keizo M, Harukazu Y and Shoji A 2007 *Jpn. J. Appl. Phys.* **46** 3636
[31] Ho K O, Leung M Y, Jiang Y, Ao K P, Zhang W, Yip K Y, Pang Y Y, Wong K C, Goh S K and Yang S 2020 *Phys. Rev. Appl.* **13** 024041
[32] Chai Y, Lu P, D H, Shen J, Ma Y, Zhai K, Wang L, Shi Y, Li H, Wang W and Sun Young 2021 *Phys. Rev. B* **104** L100413
[33] Zeng H, Zhao X, Yu G, Luo X, Ma S, Chen C, Mo Z, Zhang Y, Chai Y, Shen J and Zhong Z 2022 *J. Magn. Magn. Mater.* **560** 169631
[34] Xie W, Thimmaiah S, Lamsal J, Liu J, Heitmann T W, Quirinale D, Goldman A I, Pecharsky V and Miller G J 2013 *Inorg. Chem.* **16** 9399
[35] Hori T, Shiraish H and Ishii Y 2007 *J. Magn. Magn. Mater.* **310** 1820
[36] Adams T, Chacon A, Wagner M, Bauer A, Brandl G, Pedersen B, Berger H, Lemmens P and Pfleiderer C 2012 *Phys. Rev. Lett.* **108** 237204
[37] Thessieu c, Pfleiderer C, Stepanov A N and Flouquet J 2012 *J. Phys.: Condens. Matter* **9** 6677
[38] Schütte C, Iwasaki J, Rosch A and Nagaosa N 2014 *Phys. Rev. B* **90** 174434
[39] Petrova A E and Stishov S M 2016 *Phys. Rev. B* **94** 020410
[40] Callen E and Callen H B 1965 *Phys. Rev.* **139** A455
[41] Callen E 1968 *J. Appl. Phys.* **39** 519
[42] Kindervater J, Stasinopoulos I, Bauer A, Haslbeck F X, Rucker F, Chacon A Mühlbauer S, Franz C, Garst M, Grundler D and Pfleiderer C 2019 *Phys. Rev. X* **9** 041059
[43] Yao Y, Ding B, Liang J, Li H, Shen X, Yu R and Wang W 2022 *Nat. Commun.* **13** 5991
[44] Bogatyrëv A and Metlov K 2018 *J. Magn. Magn. Mater.* **465** 743
[45] Halder M, Chacon A, Bauer A, Simeth W, Mühlbauer S, Berger H, Heinen L, Garst M, Rosch A and Pfleiderer C 2018 *Phys. Rev. B* **98** 144429
[46] Leonov A O and Pappas C 2019 *Phys. Rev. B* **99** 144410
[47] Qian F, Bannenberg L, Wilhelm H, Chaboussant G, Debeer-Schmitt L, Schmidt M, Aqeel A, Palstra T, Brück E, Lefering A, Pappas C, Mostovoy M and Leonov A 2018 *Sci. Adv.* **4** eaat7323
[48] Morikawa D, Yu X, Karube K, Tokunaga Y, Taguchi Y, Arima T and Tokura Y 2017 *Nano Lett.* **17** 1637
[49] Preißinger M, Karube K, Ehlers D, Szigeti B, Krug von Nidda H, White J S, Ukleev V, Rønnow H M, Tokunaga Y, Kikkawa A, Tokura Y, Taguchi Y and Kézsmárki I 2021 *npj Quantum Mater.* **6** 65
[50] Cheng J, Sun L, Zhang Y, Ji T, Cao R, Miao B, Zhao Y and Ding H 2024 *Chin. Phys. B* **33** 037501
[51] Liang W, Su J, Wang Y, Zhang Y, Hu F and Cai J 2023 *Chin. Phys. B* **32** 127504
[52] Luo J, Guo J, Hou Y, Wang J, Xu Y, Zhou Y, Pong P and Zhao G 2023 *Chin. Phys. Lett.* **40** 097501
[53] Shibata K, Iwasaki J, Kanazawa N, Aizawa S, Tanigaki T, Shirai M, Nakajima T, Kubota M, Kawasaki M, Park HS, Shindo D, Nagaosa N and Tokura Y 2015 *Nat. Nanotechnol.* **10** 589
[54] Deng L, Wu H, Litvinchuk A, Yuan N, Lee J, Dahal R, Berger H, Yang H and Chu C 2020 *Proc. Natl. Acad. Sci. USA* **117** 8783
[55] Crisanti M, Reynolds N, Živković I, Magrez A, Rønnow H M, Cubitt R and White J S 2020 *Phys. Rev. B* **101** 214435